


# Spatiotemporal spread of perturbations in power-law models at low temperatures: Exact results for classical out-of-time-order correlators

Bhanu Kiran S. <sup>1</sup>, David A. Huse <sup>2</sup>, and Manas Kulkarni <sup>1</sup>

<sup>1</sup>*International Centre for Theoretical Sciences, Tata Institute of Fundamental Research, Bengaluru 560089, India*

<sup>2</sup>*Department of Physics, Princeton University, Princeton, New Jersey 08544, USA*

 (Received 3 December 2020; revised 31 July 2021; accepted 23 September 2021; published 18 October 2021)

We present exact results for the classical version of the out-of-time-order commutator (OTOC) for a family of power-law models consisting of  $N$  particles in one dimension and confined by an external harmonic potential. These particles are interacting via power-law interaction of the form  $\propto \sum_{i,j=1}^N (i \neq j) |x_i - x_j|^{-k} \forall k > 1$  where  $x_i$  is the position of the  $i$ th particle. We present numerical results for the OTOC for finite  $N$  at low temperatures and short enough times so that the system is well approximated by the linearized dynamics around the many-body ground state. In the large- $N$  limit, we compute the ground-state dispersion relation in the absence of external harmonic potential exactly and use it to arrive at analytical results for OTOC. We find excellent agreement between our analytical results and the numerics. We further obtain analytical results in the limit where only linear and leading nonlinear (in momentum) terms in the dispersion relation are included. The resulting OTOC is in agreement with numerics in the vicinity of the edge of the “light cone.” We find remarkably distinct features in OTOC below and above  $k = 3$  in terms of going from non-Airy behavior ( $1 < k < 3$ ) to an Airy universality class ( $k > 3$ ). We present certain additional rich features for the case  $k = 2$  that stem from the underlying integrability of the Calogero-Moser model. We present a field theory approach that also assists in understanding certain aspects of OTOC such as the sound speed. Our findings are a step forward towards a more general understanding of the spatiotemporal spread of perturbations in long-range interacting systems.

DOI: [10.1103/PhysRevE.104.044117](https://doi.org/10.1103/PhysRevE.104.044117)

## I. INTRODUCTION

Collective behavior of many-particle systems far from equilibrium has been a central issue of interest [1–5]. In particular, the role of integrability and its breaking in the dynamical behavior of a system is of great interest from both a theoretical [6–9] and an experimental perspective [10–12]. More generally, chaos which characterises extreme sensitivity to arbitrarily small perturbations in initial conditions has been extensively studied in both classical [13,14] and quantum systems [15,16]. Recently, long-ranged systems have taken a special place as a platform for studying collective behavior and have become a promising avenue for experimental research. Notable examples of long-ranged systems include one-dimensional one-component plasma [17–20], Dyson’s log gas [21], Calogero-Moser systems [22–24], dipolar Bose gas [25,26], ionic systems [27–29], three-dimensional Coulomb gas confined in one dimension [30], and Yukawa gas [31] to name a few. Two main ingredients for understanding sensitivity to initial conditions in long-ranged systems are (1) the availability of a family of long-ranged models which contain in them both generic and integrable cases with preferably having reasonably well-understood classical and quantum limits and (2) the availability of diagnostics which can characterize dynamical phenomena and has both classical and quantum counterparts.

The Riesz gas [32,33] is one such platform which encompasses a family of long-ranged models, and we consider

the case when it is trapped in an external trapping potential. This family contains in it several models which have themselves been a subject of great interest from both a physics and mathematics perspective. Well-known examples for specific values of  $k$  include Dyson’s log gas ( $k \rightarrow 0$ ), the integrable Calogero-Moser system ( $k = 2$ ), one-dimensional one-component plasma ( $k = -1$ ), Coloumb gas confined to 1D ( $k = 1$ ), dipolar gas ( $k = 3$ ), and hard rods ( $k \rightarrow \infty$ ). The parameter  $k$  which characterizes the power-law interaction spans from “relatively long-ranged” to “relatively short-ranged” as we increase  $k$ . Recently, collective field theory [33] has been provided for the Riesz gas and its finite ranged generalization [34]. Such a collective description is an important step forward to study nonlinear hydrodynamics [35,36].

The second ingredient, i.e., a suitable diagnostic which can characterize dynamical phenomena is the classical version of the quantum out-of-time ordered correlator (OTOC) [37–43], which quantifies growth or decay of perturbations in time and their spread in space. This quantity is precisely suited to explore questions on chaos, aspects of integrability, entropy, and nonlinearity to name a few. In recent years, classical OTOC has been employed as an insightful diagnostic tool to study various extended classical systems such as classical one-dimensional spin chains [44], thermalized fluid obeying truncated Burgers equation [45], classical interacting spins on a Kagome lattice [46,47], disordered systems [48], the two-dimensional anisotropic XXZ model [49], spherical  $p$ -spin

TABLE I. Summary of key results ( $k > 1$ ). Note that  $\alpha_k, \beta_k, \delta_k, \gamma_3$  are all given in Eq. (5).

Asymptotic Scaling of $D(x, t)$ , for large $\eta_{\pm}$ or $\Delta_{k,\pm}$	$1/x^{2k+2}$
Spread of perturbations	Ballistic
Dispersion relation, $\omega_k(q)$	$\alpha_k q - \beta_k q^k$ , for $1 < k < 3$ $\alpha_k q + \gamma_3 q^3 \log(qa)$ , for $k = 3$ $\alpha_k q - \delta_k q^3 - \beta_k q^k$ , for $3 < k < 5$
Profile of the envelope of perturbations	Convex for $k < 2$ Flat for $k = 2$ Concave for $k > 2$

glass model [50], discrete nonlinear Schrödinger equation [51], and open systems such as the driven-dissipative duffing chain[52]. The classical OTOC shines light on how perturbations spread in space and grow and decay in time. The more conventional ways of probing classical perturbations such as Lyapunov exponents can be deduced from OTOC, although the OTOC is well suited for probing extended many-particle systems.

It is worth noting that, to the best of our knowledge, all works on classical OTOC so far have been restricted to the case of short-ranged interactions (essentially nearest neighbor) and away from any integrable points [44–49,51,52]. In fact, even for short-ranged models, although there have been studies of OTOC in quantum integrable systems [43,53–57], there has been no work reported on OTOC in classical integrable models to the best of our understanding. In this work, we aim to fill this important gap in our understanding by studying low temperature OTOC of a family of power-law models. Our key results can be summarized as follows: (1) We found exact analytical computation of the dispersion relation in absence of external harmonic potential and utilized it to compute analytical results for OTOC at low temperatures and short enough times. (2) We performed direct numerics and demonstrated excellent agreement with the results obtained after using dispersion relation. (3) We obtained exact results for OTOC at the integrable point ( $k = 2$ ). (4) We introduced a field theory approach that paved an alternate path to the investigative aspects of OTOC. A summary of key results is presented in Table I.

## II. MODEL AND DEFINITIONS

We consider  $N$  classical particles in one dimension with pairwise interaction confined by an external harmonic trap. This is the so-called Riesz gas [32] given by

$$H = \sum_{i=1}^N \frac{p_i^2}{2m} + V_k(\{x_j\}), \quad (1a)$$

$$V_k(\{x_j\}) = \sum_{i=1}^N \left[ \frac{m\omega^2}{2} x_i^2 + \frac{J}{2} \sum_{j \neq i} \frac{1}{|x_i - x_j|^k} \right]. \quad (1b)$$

Here  $x_i$  is the position of the  $i$ th particle (such that  $i < j \iff x_i < x_j$ , i.e., ordering is maintained),  $p_i$  is the corresponding conjugate momentum,  $m$  is the mass of each particle,  $J$  is the interaction strength, and  $\omega$  is the frequency of the external trap. Therefore, equations of motion become

$$\dot{x}_i = p_i/m \text{ and}$$

$$\dot{p}_i = -m\omega^2 x_i + \frac{Jk}{2} \sum_{j \neq i} \frac{\text{sgn}(x_i - x_j)}{|x_i - x_j|^{k+1}}. \quad (2)$$

For a set of initial conditions  $\{x_i(0), p_i(0)\}$ , one can in principle solve the above  $N$  ordinary differential equations each consisting of  $(N - 1)$  pairing terms thereby rendering it highly nonlocal and nonlinear.

## III. DISPERSION RELATION

In the ground state in the absence of external trap, we find the dispersion relation (using small oscillation analysis) to be (Appendix B),

$$\omega_k(q) = \sqrt{\frac{Jk(k+1)}{ma^{k+2}} [2\zeta(k+2) - P(k, q)]}, \quad (3)$$

where  $P(k, q) = L_{k+2}(e^{-iqa}) + L_{k+2}(e^{iqa})$  with  $L_n(z) = \sum_{p=1}^{\infty} z^p/p^n$  being the polylogarithm function. Here  $a$  is the lattice spacing or inverse density [i.e., equilibrium is achieved when  $x_i(t) = ai$  and  $p_i(0) = 0$ ] and  $\zeta(z) = \sum_{n=1}^{\infty} 1/n^z$  is the Riemann  $\zeta$  function. The lattice spacing  $a$  can be introduced in the following manner. Let us say that we have  $N$  particles confined in a harmonic trap of frequency  $\omega$ . The minimum energy configuration is such that the density takes a dome shape [33], and the interparticle distance at the center is given by [33]  $a = 2^{\frac{3k+4}{k^2+2k}} [J(k+1)\zeta(k)/m]^{\frac{1}{k+2}} \left(\frac{\omega N}{B[1+\frac{1}{k}, 1+\frac{1}{k}]}\right)^{-\frac{2}{k+2}}$

where  $B[a, b] = \int_0^1 dw w^{a-1} (1-w)^{b-1}$  is the standard  $\beta$  function. The homogeneous limit can be thus realized by simultaneously taking a careful limit  $N \rightarrow \infty$  and  $\omega \rightarrow 0$  keeping  $\omega N$  to be a constant. For a finite  $\omega$ , the dome shape survives in the large- $N$  limit.

It turns out that the above dispersion relation [Eq. (3)] is periodic with period  $2\pi/a$ , and it has a maxima at  $q = \pi/a$ . Using the remarkable property of the polylogarithm function [58],  $L_n(z) = \Gamma(1-n) \log(1/z)^{n-1} + \sum_{l=0}^{\infty} \zeta(n-l) \frac{\log(z)^l}{l!}$  for  $n \notin \mathbb{Z}$  and  $|\ln z| < 2\pi$ , we find that the above exact dispersion relation [Eq. (3)] for  $k > 1$  has the following small- $q$  expansion up to the next leading relevant order (Appendix B):

$$\omega_k(q) \approx \begin{cases} \alpha_k q - \beta_k q^k, & 1 < k < 3 \\ \alpha_k q + \gamma_3 q^3 \log(qa), & k = 3 \\ \alpha_k q - \delta_k q^3 - \beta_k q^k, & 3 < k < 5 \end{cases} \quad (4)$$

with

$$\begin{aligned}\alpha_k &= \sqrt{\frac{Jk(k+1)}{ma^k}} \zeta(k), \quad \gamma_3 = \frac{1}{4} \sqrt{\frac{Ja}{3m\zeta(3)}}, \\ \delta_k &= \frac{1}{24} \sqrt{\frac{Jk(k+1)}{m\zeta(k)}} \frac{\zeta(k-2)}{a^{(k-4)/2}}, \\ \beta_k &= \sqrt{\frac{Jk(k+1)}{m\zeta(k)}} \cos\left[\frac{\pi}{2}(k+1)\right] a^{k/2-1} \Gamma(-1-k),\end{aligned}\quad (5)$$

where  $\Gamma(z)$  is the  $\Gamma$  function. If  $k \in \mathbb{Z}$  one can resort to the conventional definition of the polylogarithm function to get the above small- $q$  expansion (Appendix B). Note also that in the regime  $3 < k < 5$ , we wrote the next-to-next-leading-order term [Eq. (4)] since this is what remarkably results in power-law asymptotic behavior of the OTOC to be discussed later, and hence, it is a relevant term.

#### IV. OUT-OF-TIME-ORDER COMMUTATOR (OTOC)

The key diagnostic for us is the classical version of the well-known quantum OTOC. In the Heisenberg picture, the quantum OTOC can be defined [44,59] as  $D(x, t) = \langle [\hat{A}_x(t), \hat{B}_0(0)]^2 \rangle$  where  $\hat{A}_x(0)$  and  $\hat{B}_0(0)$  are local operators at position  $x$  and the origin, respectively. The average  $\langle \cdot \rangle$  is over a given quantum state. This quantity captures the effect of an operator  $\hat{B}_0(0)$  on another operator  $\hat{A}_x(t)$  at a different position and time. We now replace the commutator by a Poisson bracket,  $\{\mathcal{A}_x(t), \mathcal{B}_0(0)\}$ . For our purposes, if one makes the identification,  $\mathcal{A}_x(t) \equiv x_i(t)$  and  $\mathcal{B}_0(0) \equiv p_0(0)$ , then the Poisson bracket is  $\{x_i(t), p_0(0)\} \approx \frac{\delta x_i(t)}{\delta x_0(0)}$ . Therefore, the classical OTOC in our variables becomes  $D(i, t) = \langle \{x_i(t), p_0(0)\}^2 \rangle \approx \langle \left(\frac{\delta x_i(t)}{\delta x_0(0)}\right)^2 \rangle$ . Here  $\langle \cdot \rangle$  is the average over a thermal ensemble of initial conditions at a given temperature  $T$ . However, for low enough temperatures ( $k_B T \ll J/a^k$  where  $k_B$  is the Boltzmann constant), the initial conditions are very close to the true ground state (global minima) which is characterized by the set  $\{x_i(0) = y_i, p_i(0) = 0\}$  that minimizes the energy in Eq. (1). Therefore, for low enough temperature we do not need to make an ensemble average.  $D(i, t)$  can be interpreted as follows: Take two copies ( $I, II$ ) of a system with identical initial conditions. Now, we infinitesimally perturb the position (by  $\epsilon$ ) of one particle (say, the middle one) in only one of the copies. In such a case, the OTOC is

$$D(i, t) = \left| \frac{x_i^I(t) - x_i^{II}(t)}{x_{\frac{N+1}{2}}^I(0) - x_{\frac{N+1}{2}}^{II}(0)} \right|^2 = \left| \frac{\delta x_i(t)}{\epsilon} \right|^2, \quad (6)$$

where we assume  $N$  is an odd integer just for convenience. Since here we are in a regime of sufficiently low temperature, one can invoke a Hessian description, which yields  $|\delta \dot{\mathbf{x}}(t)\rangle = -\mathbf{M} |\delta \mathbf{x}(t)\rangle$  where  $|\delta \mathbf{x}(t)\rangle$  is a  $N \times 1$  column vector consisting of elements  $\delta x_i(t)$  and  $\mathbf{M}$  is a  $N \times N$  Hessian matrix given by  $\mathbf{M}_{ij} = \left[ \frac{\partial^2 V_k}{\partial x_i \partial x_j} \right]_{\mathbf{x}=\mathbf{y}}$  where  $\mathbf{y}$  is the equilibrium solution that minimizes Eq. (1). In this Hessian limit, Eq. (6) becomes (Appendix A)

$$D(i, t) = \left| \sum_{\alpha=1}^N \left\langle \lambda_\alpha \left| \frac{N+1}{2} \right\rangle \langle \mathbf{e}_i | \lambda_\alpha \rangle \cos(\omega_\alpha t) \right\rangle \right|^2, \quad (7)$$

where  $|\lambda_\alpha\rangle$  is the  $\alpha$ th eigenvector of  $\mathbf{M}$  and  $\omega_\alpha^2$  is the corresponding eigenvalue. The set  $\{|\mathbf{e}_i\rangle\}$  is the standard basis for  $\mathbb{R}^N$ . We have chosen the initial conditions,  $\langle \mathbf{e}_i | \delta \mathbf{x}(t=0) \rangle = \epsilon \delta_{i, \frac{N+1}{2}}$  and  $\langle \mathbf{e}_i | \dot{\delta \mathbf{x}}(t=0) \rangle = 0$  such that  $D(i, 0) = \delta_{i, \frac{N+1}{2}}$ . In general, neither the equilibrium positions  $\{y_i\}$  nor the eigenvectors and eigenvalues are easy to find. Barring the exceptional integrable case [60] of  $k=2$ , we resort to direct numerics.

#### V. DIRECT NUMERICS

In order to compute the OTOC [Eq. (7)] numerically, we first need to find the set  $\{y_i\}$ . This is done via the Broyden-Fletcher-Goldfarb-Shanno (BFGS) algorithm [61,62] which is an efficient way for energy minimization of Eq. (1) when  $N$  is large (Appendix E). All numerical results presented here are for  $N=4097$ . After getting the positions of the minima ( $\{y_i\}$ ) one can compute the Hessian matrix  $\mathbf{M}$ , its eigenvectors ( $|\lambda_\alpha\rangle$ ) and eigenvalues ( $\omega_\alpha^2$ ) thereby aiding the computation of OTOC [Eq. (7)]. It is also important to mention that for sufficiently large  $N$  the resulting density profile is sufficiently flat near the center. Hence, for comparing these direct numerical results with analytics (discussed later), we can ignore the harmonic trap as long as we are studying features relatively far from the edges.

#### VI. ANALYTICAL APPROACH

The dispersion relation [Eq. (3)], along with a plane-wave ansatz (Appendix C), gives us [52],

$$D(x, t) = \left| \frac{a}{2\pi} \int_{-\frac{\pi}{a}}^{\frac{\pi}{a}} dq \cos(qx - \omega_k(q)t) \right|^2, \quad (8)$$

where  $\omega_k(q)$  is the full dispersion relation given in Eq. (3). It is to be noted that the limits of the integral are chosen to be where the dispersion relation reaches a maximum (zero group velocity). Equation (8) encodes both the left and the right movers. In other words, Eq. (8) can be split into two pieces of integral comprising negative  $(-\pi/a, 0)$  and positive  $(0, \pi/a)$  momentum. Next, we will present the results for various values of  $k$ . Owing to a rich mathematical structure rooted in integrability, we will present the  $k=2$  case first.

$k=2$  (*Integrable Calogero-Moser Model*): It remarkably turns out that, when  $k=2$ , the expansion of Eq. (3) in  $q$  terminates to exactly yield,  $\omega_2(q) = \sqrt{\frac{J}{m} \left( \frac{\pi q}{a} - \frac{q^2}{2} \right)}$ . Using this, the OTOC Eq. (8) gives (Appendix D),

$$D(x, t) = \left| \frac{a}{2\pi} [D_R(x, t) + D_L(x, t)] \right|^2, \quad (9)$$

where  $D_L/D_R$  are the left and right moving perturbations respectively and are given by

$$\begin{aligned}D_{R,L} &= \frac{\sqrt{\pi}}{tu_t} \cos\left(\frac{\eta_{\mp}^2}{2u_t^2}\right) \left[ \pm \mathcal{C}\left(\frac{v}{u_t \sqrt{\pi}}\right) \mp \mathcal{C}\left(\frac{\eta_{\mp}}{u_t \sqrt{\pi}}\right) \right] \\ &+ \frac{\sqrt{\pi}}{tu_t} \sin\left(\frac{\eta_{\mp}^2}{2u_t^2}\right) \left[ \pm \mathcal{S}\left(\frac{v}{u_t \sqrt{\pi}}\right) \mp \mathcal{S}\left(\frac{\eta_{\mp}}{u_t \sqrt{\pi}}\right) \right],\end{aligned}\quad (10)$$

where  $u_t = (\sqrt{J}/\sqrt{mt})^{1/2}$  and  $\mathcal{C}(y)$  and  $\mathcal{S}(y)$  are the Fresnel cosine and Fresnel sine integrals, respectively (Appendix D). Here  $v = x/t$  and  $\eta_{\pm} = v \pm \sqrt{J/m}(\pi/a)$ . The velocities  $\eta_+$  and  $\eta_-$  are indeed the velocities of the fronts at right and left, respectively. The notation  $u_t$  is introduced for convenience and one can infer that  $u_t$  dictates the length scale of the oscillations as it appears inside the Fresnel functions as well as in the overall amplitude. In Fig. 1 we show the OTOC for the case  $k = 2$ . Exact agreement between direct numerics [Eq. (7)] and analytical expression [Eq. (9)] is established in Fig. 1(c). The slope of the heat map [Fig. 1(b)] is precisely the butterfly velocity (which in this ground-state case is the sound speed) given by  $v_B = \pi/a$ . This is consistent with the position of the front in Fig. 1(c), which occurs at  $v_B\tau$ . Extensive asymptotic analysis of Eq. (9) and Eq. (10) is presented in Appendix D. For example, we have shown that the right moving perturbation front has the asymptotic behavior  $D_R(t) \sim 1/\eta_-^3$  for large  $\eta_- > 0$ .

The oscillatory nature of the spatial profiles indicate that the dynamics is well approximated by a Hessian theory of small oscillations. The approximate dynamics is similar to the dynamics of an all-to-all connected Harmonic graph. The oscillatory nature is a testimony to the fact that chaos is not yet prevalent. In other words, there is no exponential temporal growth of perturbations. Remarkably, we find that the form of the envelope is a good demarcator of various  $k$  regimes (see Table I). The envelope is convex, flat and concave for  $k < 2$  [Fig. 2(a)],  $k = 2$  [Fig. 1(c)], and  $k > 2$  [Fig. 3(c)], respectively. Physically, the envelope gives us an idea of how an initial energy packet is distributed in space for various values of  $k$ .

Although the exact analytical form of the OTOC for  $k \neq 2$  is not available due to the complexity of the dispersion relation [Eq. (3)], significant advance can be made due to the small- $q$  expansion [Eq. (4)], which is what we do next.

*Nonintegrable case,  $k \neq 2$ :* For the case of  $k \neq 2$ , one can compare the direct numerical simulations of Eq. (7) with the analytical expression in Eq. (8) with  $\omega_k(q)$  given by Eq. (3). In Fig. 2 we present an example for  $k = 1.5$ . We see perfect agreement in entire space-time. However, given the complexity of  $k \neq 2$  case, we do not have an analog of Eq. (9) and Eq. (10), which assumed a fully exact dispersion relation which takes a remarkably simple form in the Calogero-Moser ( $k = 2$ ) case. We therefore resort to a small- $q$  expansion of Eq. (3). We recollect that such an expansion gave us Eq. (4) along with definitions given in Eq. (5). Note that such an expansion is expected to work close to a particular front (either right or left). Therefore, in the following discussions, we will restrict ourselves to the right sector, and our analysis straightforwardly holds for the left sector. We will discuss three cases in Eq. (4) separately.

$1 < k < 3$  : Here we simplify Eq. (8) using the first line of Eq. (4). Doing so, we get (Appendix D)

$$D_R(x, t) = \frac{a}{2\pi} \frac{B_k(\Delta_{k,-})}{(3t\beta_k)^{1/k}}, \quad \text{with } \Delta_{k,-} = \frac{x - \alpha_k t}{(3t\beta_k)^{1/k}}, \quad (11)$$

and the special function is defined as (for  $1 < k < 3$ )

$$B_k(y) := \int_0^{(3t\beta_k)^{1/k} \frac{\pi}{a}} ds \cos\left(y s + \frac{s^k}{3}\right). \quad (12)$$

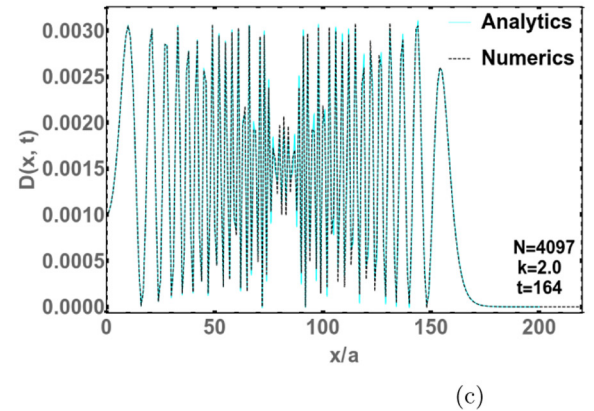
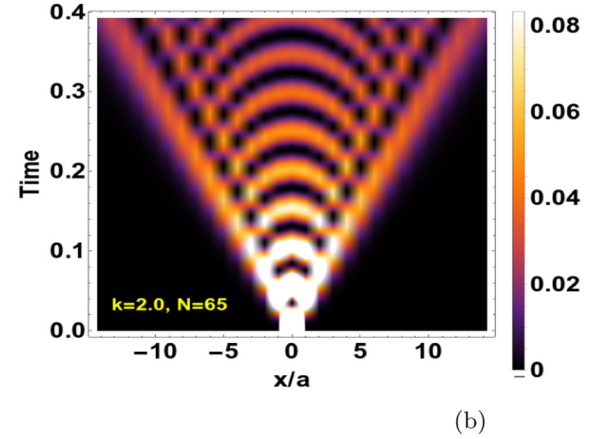
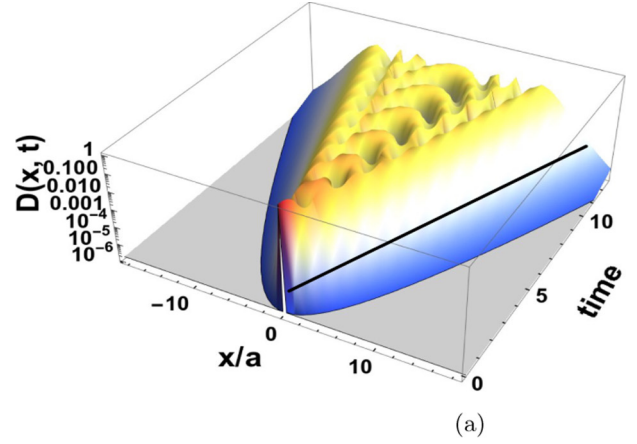


FIG. 1. (a) Heat map of the OTOC (for clear visualization, we chose  $N = 65$ ) from direct numerical simulation of Eq. (7) for the Calogero-Moser case ( $k = 2$ ). The solid black line separating the white and blue (gray) regions depicts the light cone. Time axis is in units of  $a/v_B$ . (b) 2D heat map showing a ballistic light cone ( $N = 65$ ). Note that each point in the plot corresponds to the amplitude of the OTOC. (c) Comparing OTOC from direct numerical simulation of Eq. (7) with the analytical expression in Eq. (9) at a time snapshot,  $t \approx 164$  (in units of  $a/v_B$ ). Note that, for visualization purposes, we have plotted only the positive  $x$ -axis, and the results are mirror symmetric on the other side. The time  $t$  is chosen such that the front moves about 10% from the center to make sure that we are far enough from the edge of the cloud. Here  $a = 0.0347$ ,  $v_B = 90.5207$

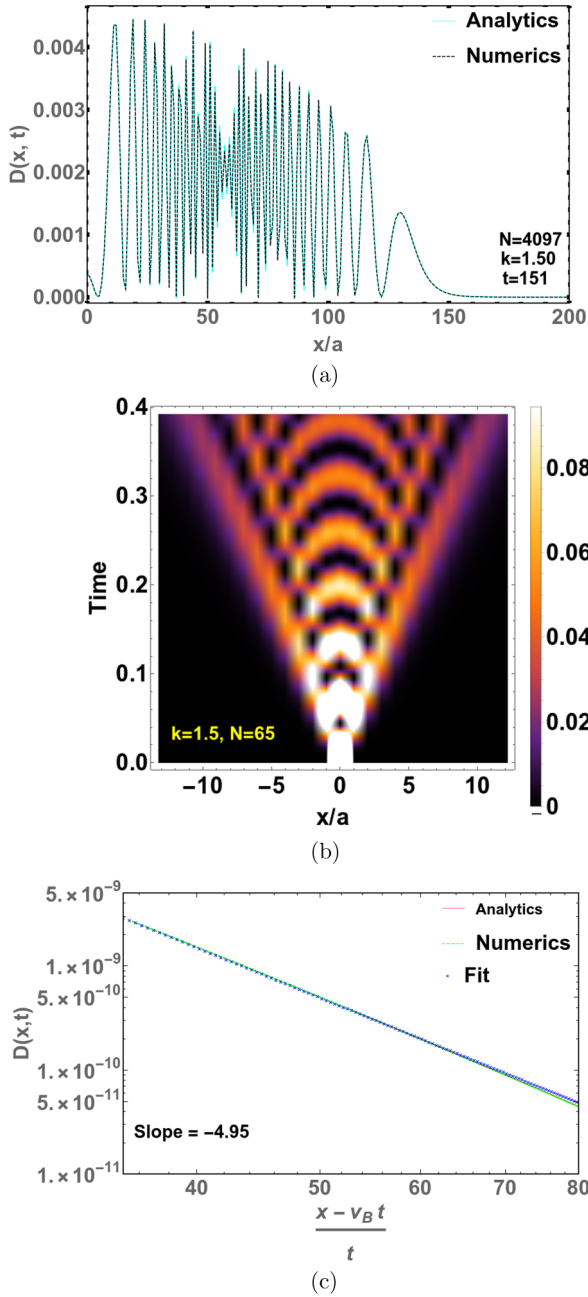


FIG. 2. (a) Comparing OTOC ( $k = 1.5$ ) from direct numerical simulation of Eq. (7) with the analytical expression in Eq. (8) at a time snapshot,  $t \approx 151$  (in units of  $a/v_B$ ). Note again that, for visualization purposes, we have plotted only the positive  $x$ -axis and the results are mirror symmetric on the other side. The time  $t$  is again chosen such that the front moves about 10% from the center to make sure that we are far enough from the edge. Note the difference in the profiles of the OTOC. While  $k = 2$  has a relatively flat envelope [Fig. 1(c)],  $k = 1.5$  shows a downward trending envelope and  $k = 4.5$  has an upward trending envelope (Appendix C). (b) 2D heat map showing a ballistic light cone. (c) Log-log plot showing the asymptotic power-law behavior for  $k = 1.5$ . This plot is the zoomed version of the plot in the top panel near the right front, with  $x \in [5.5, 8.5]$ . Here  $a \sim 0.02237$  and  $v_B \sim 53.9296$ .

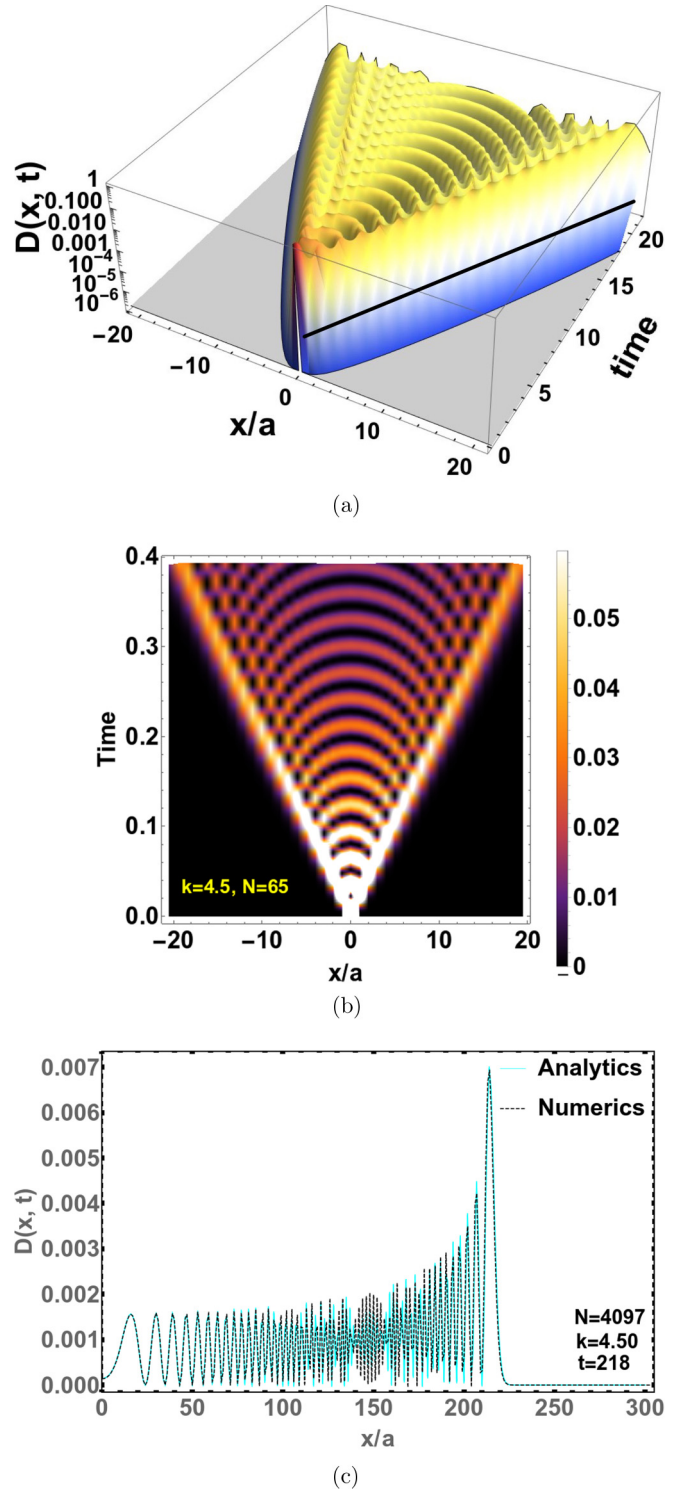


FIG. 3. (a) Heat map of the OTOC, for  $k = 4.5$  and  $N = 65$ , from direct numerical simulations. The time axis is in units of  $a/v_B$ . The solid black line separating the white and blue (gray) regions depicts the light cone. (b) 2D heat map showing a ballistic light cone. (c) Comparing OTOC from direct numerical simulation with the analytical expression at a time snapshot,  $t \approx 218$  (in units of  $a/v_B$ ). Note that, for visualization purposes, we have plotted only the positive  $x$ -axis and the results are mirror symmetric on the other side. Here  $a \sim 0.1346$ ,  $v_B \sim 466.514$ .

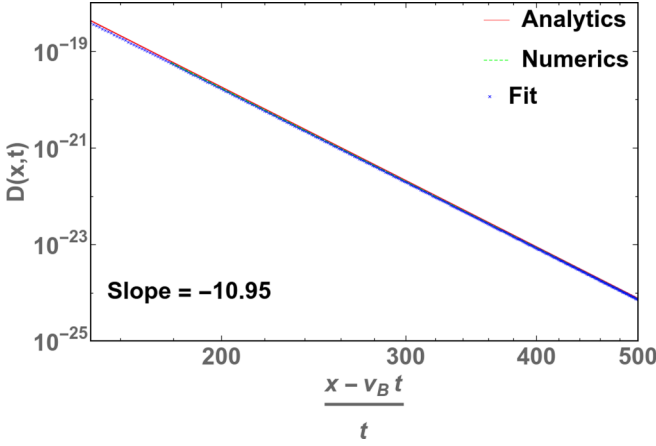


FIG. 4. Power-law decay of OTOC beyond the cone for  $k = 4.5$  and  $N = 4097$ . The slope depicts the exponent of the power law. Here  $a \sim 0.1346$ ,  $v_B \sim 466.514$ .

Equation (16) below expresses  $\Delta_{k,\pm}$  for various values of  $k$ . Note that when the lattice spacing  $a \rightarrow 0$  (which is essentially the large- $N$  limit), then the upper limit of the integral in Eq. (12) becomes  $+\infty$ . This can be thought of as a  $k \neq 3$  generalization of the Airy integral. In stark contrast to the Airy integral, in the regime  $1 < k < 3$ , we find  $B_k(y) \sim 1/y^{k+1}$  for large  $y$ . This implies that  $D_{L,R}(x,t) \propto 1/\Delta_{\pm}^{k+1}$  where  $\pm$  indicates whether we are probing the left or the right front, respectively. Note that, throughout the paper, for the sake of brevity by  $\Delta_{\pm}$  we mean  $\Delta_{k,\pm}$ . In Fig. 2(c) we demonstrate that this power-law prediction (for  $k = 1.5$  which will give  $D \sim 1/\Delta_{\pm}^5$ ) is consistent with direct numerical results.

$3 < k < 5$ : In this case, if we consider the lowest and the next-order term in the dispersion relation [Eq. (4)] we get

$$D_R(x,t) = \frac{a \text{Ai}(\Delta_{k,-})}{2(3t\delta_k)^{1/3}}, \quad \text{with } \Delta_{k,-} = \frac{x - \alpha_k t}{(3t\delta_k)^{1/k}}, \quad (13)$$

where  $\text{Ai}(z)$  is the Airy function. Refer to Eq. (16) to see the definition of  $\Delta_{k,\pm}$  in various regimes of  $k$ . This would imply that the asymptotic behavior of the OTOC [Eq. (8)] would be characterized by exponential since large argument behavior of the Airy function is  $\text{Ai}(z) \sim \frac{e^{-\frac{2}{3}z^{3/2}}}{2\sqrt{\pi}z^{1/4}}$ . However, this is because we stopped at  $O(q^3)$  in Eq. (4). Knowing that we have a power-law model, we expect that the asymptotic behavior of OTOC should be characterized by power laws. It turns out that this is captured by considering higher orders in the dispersion relation [Eq. (8)]. For  $3 < k < 5$ , the next-order term after  $q^3$  in Eq. (4) would be  $q^k$  and this will yield a power-law tail  $D_{L,R}(x,t) \propto 1/\Delta_{\pm}^{k+1}$ . For example, for the case  $k = 4.5$  (see Fig. 3), we demonstrate (Appendix D) that  $D_{L,R}(x,t) \propto 1/\Delta_{\pm}^{5.5}$  (see Fig. 4).

We briefly comment on the case  $5 < k < \infty$  and  $k \notin \text{odd integer}$ . The term in the dispersion expansion that results in power law is  $\delta_k q^k$ , which will again yield  $D_{L,R}(x,t) \propto 1/\Delta_{\pm}^{k+1}$ . However, to see this power law, one needs to go to very large asymptotic values since this will happen only after all the exponential behaviours [arising due to  $O(q^{2\mathbb{Z}+1})$  where  $\mathbb{Z}$  are positive integers] are suppressed. Next, we will discuss the case when  $k$  is an odd integer. In particular, we will discuss

the case of  $k = 3$ , but our method can be adapted for all odd integers.

$k = 3$ : In this case, we see a logarithm term in Eq. (4), i.e.,  $q^3 \log(q)$ . Note that without the logarithmic piece, we would have ended up with Airy function for the OTOC, which would have resulted in exponential asymptotics. However, we now get

$$D_R(x,t) = \frac{a}{2\pi} \frac{B_3(\Delta_{k,-})}{(3t\gamma_3)^{1/3}}, \quad (14)$$

where

$$B_3(y) := \int_0^{(3t\gamma_3)^{1/3} \frac{\pi}{a}} ds \cos\left(y s + \frac{s^3}{3} \log\left[\frac{s}{(3t\gamma_3)^{1/3}}\right]\right). \quad (15)$$

We find that the large  $y$  behavior is  $B_3(y) \sim 1/y^4$ , which implies  $D_{L,R}(x,t) \propto 1/\Delta_{\pm}^4$ . It is remarkable to note that the expected power-law behavior is recovered as a result of the intricate role played by the logarithmic term in the dispersion relation for  $k = 3$ . We also find that for odd integers, i.e.,  $k \in 2\mathbb{Z} + 1$  where  $\mathbb{Z}$  are positive integers, the power law is recovered by a term in the dispersion relation of the form  $\beta_k q^k \log(q)$ .

It is worth recollecting that the details of  $\Delta_{\pm} \equiv \Delta_{k,\pm}$  depends on the regime of  $k$  we are investigating. This is summarized as follows:

$$\Delta_{\pm} = \begin{cases} \frac{x \pm \alpha_k t}{(3t\beta_k)^{1/k}}, & 1 < k < 3 \\ \frac{x \pm \alpha_k t}{(3t\gamma_3)^{1/3}}, & k = 3 \\ \frac{x \pm \alpha_k t}{(3t\delta_k)^{1/k}}, & 3 < k < 5 \end{cases}. \quad (16)$$

## VII. FIELD THEORY

An alternative approach to studying the large  $N$  behavior of this system is to investigate the collective field theory. Recently, a systematic derivation of large- $N$  field theory [33] was achieved. Here we will show that certain aspects of spatiotemporal spread of correlations such as the butterfly velocity can be obtained by a field theory. Let us define a density field,  $\rho(x) = \sum_{i=1}^N \langle \delta(x - x_i) \rangle$ , where  $\langle \cdot \rangle$  denotes an average with respect to a Boltzmann measure. We also define a momentum field,  $j(x) = \sum_{i=1}^N \langle p_i \delta(x - x_i) \rangle$ . We will introduce a velocity field  $v(x)$  such that  $j(x) = \rho(x)v(x)$ . In large  $N$  at sufficiently low temperatures, the field theory is given by,  $H[\rho_N(x)] \approx \frac{m}{2} \int \rho(x)v(x)^2 dx + J\zeta(k) \int \rho(x)^{k+1} dx$ . This in conjunction with Poisson brackets,  $\{\rho(x_1), v(x_2)\} = \frac{1}{m} \delta'(x_1 - x_2)$ , gives

$$\dot{\rho} = -\partial_x(\rho v), \quad \dot{v} = -\partial_x \left[ \frac{v^2}{2} + \frac{J}{m} \zeta(k)(k+1)\rho^k + \dots \right]. \quad (17)$$

One can linearize the above continuity and Euler equations by using  $\rho(x,t) = \rho_0 + \delta\rho(y,t)$ ,  $v(x,t) = 0 + \delta v(x,t)$  to get a wave equation with sound speed given by  $c = \sqrt{(J/m)k(k+1)\zeta(k)\rho_0^k}$ . This is precisely the butterfly velocity in agreement with  $\alpha_k$  given in Eq. (5). The background density ( $\rho_0$ ) and the inverse lattice spacing ( $a^{-1}$ ) have already been discussed.

### VIII. CONCLUSIONS

In summary, we studied a family of power-law models at low temperature. In particular, we probed in detail the spatiotemporal spread of perturbations. We could analytically compute the dispersion relation in absence of external harmonic potential and utilize it to get analytical results for OTOC at low temperatures. We then performed direct numerics with the aid of BFGS algorithm and demonstrated excellent agreement with the results obtained after using the dispersion relation. Exact results for OTOC at the integrable point ( $k = 2$ ) were obtained. We also presented a collective field theory approach to understand certain features of the OTOC such as the butterfly speed. The main observations are summarized in Table I.

Our work was restricted to low enough temperatures and short enough times so that the system is still in the linear regime. Therefore, although there was spread of perturbations, we restricted ourselves to temperatures and timescales where there was no growth in magnitude of perturbations. Precisely quantifying the limits of this regime as well as exploring beyond it is part of our planned future work. It is worth noting that for the temperature range considered in our paper, the quantum analog would be the probe of the ground state [63–65] rather than chaos. Being a long-ranged system of particles, high-temperature studies are considerably numerically intense, and it will be interesting to study classical OTOC and the largest Lyapunov exponent using methods of Ref. [66]. In such high-temperature cases one expects exponential (non-integrable,  $k \neq 2$ ) or power-law (integrable,  $k = 2$ ) growth, and this will be addressed in a future work. Understanding aspects of integrability ( $k = 2$ ) and its breaking through the lens of OTOC still remains largely unexplored and is an interesting future direction. The analogous quantum case is a fascinating and challenging problem especially given the fact that quantum long-ranged systems exhibit rich OTOC features depending on the exponent ( $k$ ) of the power-law interactions [67]. Needless to mention, the comparison with the quantum case should be done with caution. Nonetheless, a linear light cone is predicted in both our results (classical case) and Ref. [67] ( $T = \infty$  quantum case) for the exponent  $k > 1$ . This is remarkable and unexpected especially given the fact that these are quite different models thereby hinting towards an underlying universality.

### ACKNOWLEDGMENTS

We would like to thank A. Dhar, A. Kundu, and A. K. Chatterjee for useful discussions. M.K. would like to acknowledge support from the project 6004-1 of the Indo-French Centre for the Promotion of Advanced Research (IFCPAR), Ramanujan Fellowship (SB/S2/RJN-114/2016), SERB Early Career Research Award (ECR/2018/002085), and SERB Matrics Grant (MTR/2019/001101) from the Science and Engineering Research Board (SERB), Department of Science and Technology, Government of India. D.H. is supported in part by (USA) DOE grant DE-SC0016244. B.K.S. and M.K. acknowledge support of the Department of Atomic Energy, Government of India, under Project no. RTI4001. M.K. thanks the hospitality of the Department of Physics, Princeton University where some of the work was done.

### APPENDIX A: OTOC IN HESSIAN APPROXIMATION VALID IN THE LOW- $T$ REGIME

Here we present a derivation of the OTOC in the Hessian approximation. Let us recap that the Hamiltonian is given by

$$H = \sum_{i=1}^N \frac{p_i^2}{2m} + V_k(\{x_j\}), \quad (\text{A1a})$$

$$V_k(\{x_j\}) = \sum_{i=1}^N \left[ \frac{m\omega^2}{2} x_i^2 + \frac{J}{2} \sum_{j \neq i} \frac{1}{|x_i - x_j|^k} \right], \quad (\text{A1b})$$

which therefore yields the  $N \times N$  Hessian matrix,

$$\mathbf{M}_{ij} = \left[ \frac{\partial^2 V_k}{\partial x_i \partial x_j} \right]_{\mathbf{x}=\mathbf{y}}, \quad (\text{A2})$$

where  $\mathbf{y}$  is the equilibrium solution that minimizes Eq. (A1). Let us define a column vector ( $N \times 1$ ) representing the relative displacement (again a  $N \times 1$  column vector) of corresponding particles of copy  $I$  and copy  $II$ :

$$|\delta \mathbf{x}(t)\rangle = |\mathbf{x}^I(t)\rangle - |\mathbf{x}^{II}(t)\rangle. \quad (\text{A3})$$

Let  $\mathbf{M}$  be the Hessian matrix. We therefore have

$$|\delta \ddot{\mathbf{x}}(t)\rangle = -\mathbf{M} |\delta \mathbf{x}(t)\rangle. \quad (\text{A4})$$

We assume initial condition for velocities  $\langle \mathbf{e}_i | \delta \dot{\mathbf{x}}(t=0) \rangle = 0$  where  $\{|\mathbf{e}_i\rangle\}$  is the standard basis for  $\mathbb{R}^N$ . Let  $|\lambda_\alpha\rangle$  be the eigenvectors and  $\omega_\alpha^2$  be the corresponding eigenvalues of  $\mathbf{M}$ . In the eigenbasis, the solution is

$$|\delta \mathbf{x}(t)\rangle = \sum_{\alpha=1}^N \langle \lambda_\alpha | \delta \mathbf{x}(0) \rangle |\lambda_\alpha\rangle \cos(\omega_\alpha t). \quad (\text{A5})$$

With our chosen initial condition  $\langle \mathbf{e}_i | \delta \mathbf{x}(0) \rangle = \epsilon \delta_{i, \frac{N+1}{2}}$  the OTOC finally becomes

$$D(i, t) = \left| \frac{\langle \mathbf{e}_i | \delta \mathbf{x}(t) \rangle}{\epsilon} \right|^2 = \left| \sum_{\alpha=1}^N \left\langle \lambda_\alpha \left| \frac{N+1}{2} \right\rangle \langle \mathbf{e}_i | \lambda_\alpha \rangle \cos(\omega_\alpha t) \right|^2. \quad (\text{A6})$$

### APPENDIX B: DERIVATION OF THE DISPERSION RELATION

Here we present a detailed derivation of the dispersion relation. Let us consider the Riesz gas [Eq. (A1)] without the harmonic trap. We will also consider the case of  $N \rightarrow \infty$  and label the particles from  $-\infty$  to  $+\infty$  without loss of generality. The corresponding equations of motion are

$$\dot{x}_i = p_i/m, \quad \dot{p}_i = \frac{Jk}{2} \sum_{j=-\infty, j \neq i}^{\infty} \frac{\text{sgn}(x_i - x_j)}{|x_i - x_j|^{k+1}}. \quad (\text{B1})$$

The equilibrium solution takes the form

$$x_i(t=0) = ia, \quad p_i(t=0) = 0, \quad (\text{B2})$$

where  $a$  is a chosen lattice spacing. The above solution [Eq. (B2)] does not evolve, and therefore it is an equilibrium solution for Eq. (B1). This is so because Eq. (B1) is an odd sum. In other words,

$$\sum_{j=-\infty}^{\infty} \sum_{j \neq i} \frac{\text{sgn}(x_i - x_j)}{|x_i - x_j|^{k+1}} = \frac{1}{a^{k+1}} \sum_{j=-\infty}^{\infty} \sum_{j \neq i} \frac{\text{sgn}(i - j)}{|i - j|^{k+1}} = 0. \quad (\text{B3})$$

Having found an equilibrium background, we do a small oscillation analysis of Eq. (B1). Using the ansatz

$$x_i(t) = ai + \epsilon \cos(qai - \omega_k t), \quad (\text{B4})$$

we get from Eq. (B1)

$$-m\omega^2 \epsilon \cos(qai - \omega t) = \frac{Jk}{2} \sum_{j \neq i} \frac{\text{sgn}(x_i - x_j)}{|a(i - j) + \epsilon[\cos(qai - \omega t) - \cos(qaj - \omega t)]|^{k+1}}. \quad (\text{B5})$$

Note that, from Eq. (B5) onwards, for convenience of notation we suppress the subscript  $k$  in  $\omega_k$ , and it is restored in the end. Also,  $\epsilon$  introduced for the small oscillation analysis in Eq. (B4) should not be confused with the  $\epsilon$  used in the definition of OTOC [Eq. (6)].

Splitting the summation above [Eq. (B5)] gives

$$\begin{aligned} -m\omega^2 \epsilon \cos(qai - \omega t) &= \sum_{j < i} \frac{Jk}{|a(i - j)|^{k+1}} \frac{1}{|1 + \frac{\epsilon}{a(i-j)}[\cos(qai - \omega t) - \cos(qaj - \omega t)]|^{k+1}} \\ &\quad - \sum_{j > i} \frac{Jk}{|a(i - j)|^{k+1}} \frac{1}{|1 + \frac{\epsilon}{a(i-j)}[\cos(qai - \omega t) - \cos(qaj - \omega t)]|^{k+1}}. \end{aligned} \quad (\text{B6})$$

Since  $\frac{\epsilon}{a} \ll 1$  (small oscillation theory), we use the binomial expansion. Remember that our choice of labeling,  $x_i < x_j \iff i < j$ , means that the absolute value can be removed once the sum is broken into parts as done in Eq. (B6). We keep terms only up to leading order in  $\epsilon$ . Simple algebra and trigonometric identities simplify the expression to give

$$\begin{aligned} m\omega^2 \cos(qai - \omega t) &= \sum_{j=-\infty}^{i-1} \frac{-2Jk(k+1)}{[a(i-j)]^{k+2}} \left[ \sin\left(qa \frac{i+j}{2} - \omega t\right) \sin\left(qa \frac{i-j}{2}\right) \right] \\ &\quad + \sum_{j=i+1}^{\infty} \frac{2Jk(k+1)}{[a(j-i)]^{k+2}} \left[ \sin\left(qa \frac{j+i}{2} - \omega t\right) \sin\left(qa \frac{j-i}{2}\right) \right]. \end{aligned} \quad (\text{B7})$$

Let us define integers  $i - j \equiv x_1$  and  $j - i \equiv x_2$  in the first and the second sum in Eq. (B7), respectively. Further simplification yields

$$\begin{aligned} m\omega^2 \cos(qai - \omega t) &= \sum_{x_1=1}^{\infty} \frac{-2Jk(k+1)}{(ax_1)^{k+2}} \left[ \sin(qai - \omega t) \cos\left(\frac{qa x_1}{2}\right) \sin\left(\frac{qa}{2} x_1\right) - \cos(qai - \omega t) \sin^2\left(\frac{qa}{2} x_1\right) \right] \\ &\quad + \sum_{x_2=1}^{\infty} \frac{2Jk(k+1)}{(ax_2)^{k+2}} \left[ \sin(qai - \omega t) \cos\left(\frac{qa}{2} x_2\right) \sin\left(\frac{qa}{2} x_2\right) + \cos(qai - \omega t) \sin^2\left(\frac{qa}{2} x_2\right) \right]. \end{aligned} \quad (\text{B8})$$

In Eq. (B8),  $x_1$  and  $x_2$  are dummy variables, and it is easy to see that the first terms in each of the sums cancels each other. The expression [Eq. (B8)] easily simplifies further to [restoring the subscript  $k$  notation from Eq. (B4)]

$$\omega_k^2(q) = \frac{4Jk(k+1)}{ma^{k+2}} \sum_{x_1=1}^{\infty} \frac{\sin^2\left(\frac{qa}{2} x_1\right)}{x_1^{k+2}}. \quad (\text{B9})$$

Using the relation  $\sin(z) = \frac{e^{iz} - e^{-iz}}{2i}$ , we see that Eq. (B9) can be simplified to

$$\omega_k(q) = \sqrt{\frac{Jk(k+1)}{ma^{k+2}} [2\zeta(k+2) - L_{k+2}(e^{-iqa}) - L_{k+2}(e^{iqa})]}, \quad (\text{B10})$$

where  $\zeta(z) = \sum_{n=1}^{\infty} 1/n^z$  is the Riemann  $\zeta$  function and  $\text{Li}_n(z) = \sum_{k=1}^{\infty} \frac{z^k}{k^n}$  is the polylogarithm function. Note that Eq. (B10) is the exact dispersion relation. Figure 1 (left) shows a plot of  $\omega_k(q)$  for  $k = 2$ . Further, using the following

remarkable identity of the polylogarithm function [58]

$$L_n(z) = \Gamma(1-n) \log(1/z)^{n-1} + \sum_{l=0}^{\infty} \zeta(n-l) \frac{\log(z)^l}{l!} \quad (\text{B11})$$



for  $n \notin \mathbb{Z}$  and  $|\ln z| < 2\pi$ , one can expand Eq. (B10) (to the next-to-next leading order) as a power series in  $q$  to obtain

$$\omega_k(q) \approx \begin{cases} \alpha_k q - \beta_k q^k - \delta_k q^3, & 1 < k < 3 \\ \alpha_k q + \gamma_3 q^3 \log(qa) - \bar{\gamma}_3 q^3, & k = 3 \\ \alpha_k q - \delta_k q^3 - \beta_k q^k, & 3 < k < 5 \end{cases} \quad (\text{B12})$$

with

$$\begin{aligned} \alpha_k &= \sqrt{\frac{Jk(k+1)}{ma^k}} \zeta(k), \quad \gamma_3 = \frac{1}{4} \sqrt{\frac{Ja}{3m\zeta(3)}}, \\ \delta_k &= \frac{1}{24} \sqrt{\frac{Jk(k+1)}{m\zeta(k)}} \frac{\zeta(k-2)}{a^{(k-4)/2}}, \\ \beta_k &= \sqrt{\frac{Jk(k+1)}{m\zeta(k)}} \cos\left(\frac{\pi}{2}[k+1]\right) a^{k/2-1} \Gamma(-1-k), \\ \bar{\gamma}_3 &= \frac{25\gamma_3}{12}. \end{aligned} \quad (\text{B13})$$

It is to be noted that, if  $k \in \mathbb{Z}$  one can resort to the conventional definition of polylogarithm function to get the above small- $q$  expansion. In Eq. (B13) we see that both  $\beta_k$  and  $\delta_k$  terms diverge in the limit  $k \rightarrow 3$ . But upon a careful computation of this limit, it is seen that these divergences in fact cancel each other and give rise to the logarithm term in the dispersion relation for  $k = 3$ . More precisely,

$$\begin{aligned} & \lim_{k \rightarrow 3} (\beta_k q^k + \delta_k q^3) \\ &= \lim_{\epsilon \rightarrow 0} (\beta_{3 \pm \epsilon} q^{3 \pm \epsilon} + \delta_{3 \pm \epsilon} q^3) \\ &= \sqrt{\frac{Ja3(4)}{m\zeta(3)}} q^3 \lim_{\epsilon \rightarrow 0} \left( q^\epsilon a^{\epsilon/2} \Gamma(-4 \mp \epsilon) + \frac{1}{24} a^{-\epsilon/2} \zeta(1 \pm \epsilon) \right) \\ &= 6 \sqrt{\frac{Ja}{3m\zeta(3)}} \left( \frac{25 - 12 \log(qa)}{288} \right) q^3 \\ &= -\gamma_3 q^3 \log(qa) + \bar{\gamma}_3 q^3. \end{aligned} \quad (\text{B14})$$

Moreover, this kind of cancellation is seen for all odd integer values of  $k$ , leading to a logarithm term  $\sim q^k \log(q)$ . This is a crucial term in the dispersion relation because this is precisely the term which leads to a power-law decay of the OTOC beyond the cone, for odd integer values of  $k$ .

### APPENDIX C: OTOC IN PLANE-WAVE BASIS FOR LARGE $N$

Here we briefly derive the large- $N$  expression of the OTOC in the plane-wave basis. Let  $|\delta \mathbf{x}(t)\rangle$  be a vector containing the displacements  $\delta x_j(t)$ . We can expand this vector in terms of the plane-wave phonons of our system as

$$|\delta \mathbf{x}(t)\rangle = \frac{a}{2\pi} \int_{-\pi/a}^{\pi/a} dq \langle q | \delta \mathbf{x}(t) \rangle |q\rangle, \quad (\text{C1})$$

which implies

$$\langle e_j | \delta \mathbf{x}(t) \rangle = \frac{a}{2\pi} \int_{-\pi/a}^{\pi/a} dq \langle q | \delta \mathbf{x}(t) \rangle \langle e_j | q \rangle, \quad (\text{C2})$$

where  $\langle e_j | \delta \mathbf{x}(t) \rangle = \delta x_j(t)$ . Here we remind that  $\{|e_i\rangle\}$  is the standard basis for  $\mathbb{R}^N$ . At  $t = 0$ , since  $\langle e_j | \delta \mathbf{x}(t = 0) \rangle = \epsilon \delta_{j,0}$  and  $\langle e_j | q \rangle = \text{Real}[e^{i(qja - \omega_k(q)t)}]$  at time  $t$ , we have  $\langle q | \delta \mathbf{x}(t = 0) \rangle = \epsilon$  (constant), which ensures that Eq. (C1) is satisfied at  $t = 0$ . The noninteracting phonons simply evolve freely, so, using  $ja \equiv x$ , we can write

$$\langle e_j | \delta \mathbf{x}(t) \rangle = \frac{\epsilon a}{2\pi} \text{Real} \left[ \int_{-\pi/a}^{\pi/a} dq e^{i[qx - \omega_k(q)t]} \right]. \quad (\text{C3})$$

We therefore finally get

$$D(x, t) = \left| \frac{\langle e_j | \delta \mathbf{x}(t) \rangle^2}{\epsilon} \right| = \left| \frac{a}{2\pi} \int_{-\pi/a}^{\pi/a} dq \cos(qx - \omega_k(q)t) \right|^2, \quad (\text{C4})$$

where  $\omega_k(q)$  is given in Eq. (B10). Figures 1(c) and 3(c) show a plot of Eq. (C4) for cases  $k = 2$  and  $k = 4.5$ , respectively. The figures show only the right sector ( $x > 0$ ), the left sector ( $x < 0$ ) being just the mirror image.

### APPENDIX D: ASYMPTOTIC ANALYSIS OF OTOC

In this appendix we provide the asymptotic analysis of the OTOC at either the left or the right front. We divide this section into  $k = 2$  (integrable case) and  $k \neq 2$  (nonintegrable case).

#### 1. Integrable case, $k = 2$

In this case, the dispersion [Eq. (B10)] remarkably has a finite expansion,

$$\omega_2(q) = \sqrt{\frac{J}{m}} \left( \frac{\pi q}{a} - \frac{q^2}{2} \right), \quad \text{for } k = 2. \quad (\text{D1})$$

This allows us to cast the OTOC in terms of the Fresnel functions without resorting to any approximations. We would like to understand the behavior of the OTOC in the large  $\eta_{\pm}$  limit where  $\eta_{\pm} = v \pm \sqrt{\frac{J}{m}} \frac{\pi}{a}$ . For example, large  $\eta_-$  means that we are probing the asymptotics of the right front. For this, we look at the asymptotics of the following equations:

$$\begin{aligned} D_{R,L} &= \frac{\sqrt{\pi}}{u_t} \cos\left(\frac{\eta_{\mp}^2}{2u_t^2}\right) \left[ \pm \mathcal{C}\left(\frac{v}{\sqrt{\pi}u_t}\right) \mp \mathcal{C}\left(\frac{\eta_{\mp}}{\sqrt{\pi}u_t}\right) \right] \\ &+ \frac{\sqrt{\pi}}{u_t} \sin\left(\frac{\eta_{\mp}^2}{2u_t^2}\right) \left[ \pm \mathcal{S}\left(\frac{v}{\sqrt{\pi}u_t}\right) \mp \mathcal{S}\left(\frac{\eta_{\mp}}{\sqrt{\pi}u_t}\right) \right], \end{aligned} \quad (\text{D2})$$

where  $\mathcal{C}(r) = \int_0^r dt \cos(\pi t^2/2)$  and  $\mathcal{S}(r) = \int_0^r dt \sin(\pi t^2/2)$  are the Fresnel cosine and sine integrals, respectively. Recall that  $u_t = \sqrt{J/\sqrt{mt}}$ .

For our purpose we use the large argument asymptotic form of Fresnel integrals. In the large  $r$  limit, we have

$$S(r) = \frac{1}{2} + \cos\left(\frac{\pi r^2}{2} + O(r^{-4})\right) \left[ -\frac{1}{\pi r} + O(r^{-4}) \right] + \sin\left(\frac{\pi r^2}{2} + O(r^{-4})\right) \left[ -\frac{1}{\pi^2 r^3} + O(r^{-4}) \right], \quad (\text{D3a})$$

$$C(r) = \frac{1}{2} + \sin\left(\frac{\pi r^2}{2} + O(r^{-4})\right) \left[ \frac{1}{\pi r} + O(r^{-4}) \right] + \cos\left(\frac{\pi r^2}{2} + O(r^{-4})\right) \left[ -\frac{1}{\pi^2 r^3} + O(r^{-4}) \right]. \quad (\text{D3b})$$

We reemphasize here that to get the correct asymptotic behavior in the right sector, we go to the large  $\eta_-$  limit. Note that  $v \gg \eta_-$ . This is because  $v = v_B + \eta_-$  and  $v_B$  is very large in the limit that lattice spacing is very small. Therefore, we can take the limit  $v \rightarrow \infty$  while assuming  $\eta_-$  to be large enough to be able to do asymptotics. We use Eqs. (D3) to get the large  $\eta_-$  expansion for  $D_R$  and set  $v\sqrt{\frac{m}{J\pi}} \rightarrow \infty$  in the argument of the Fresnel functions. This finally yields

$$D_R \approx \frac{\sqrt{2}}{u_t} \cos\left(\frac{\eta_-^2}{2u_t^2}\right) \sqrt{\frac{\pi}{8}} + \frac{\sqrt{2}}{u_t} \sin\left(\frac{\eta_-^2}{2u_t^2}\right) \sqrt{\frac{\pi}{8}} - \frac{\sqrt{2}}{u_t} \cos\left(\frac{\eta_-^2}{2u_t^2}\right) \left[ \sqrt{\frac{\pi}{8}} + \frac{\sin\left(\frac{\eta_-^2}{2u_t^2}\right)}{\sqrt{2}\eta_-/u_t} - \frac{\cos\left(\frac{\eta_-^2}{2u_t^2}\right)}{4(\eta_-/\sqrt{2}u_t)^3} \right] - \frac{\sqrt{2}}{u_t} \sin\left(\frac{\eta_-^2}{2u_t^2}\right) \left[ \sqrt{\frac{\pi}{8}} - \frac{\cos\left(\frac{\eta_-^2}{2u_t^2}\right)}{\sqrt{2}\eta_-/u_t} - \frac{\sin\left(\frac{\eta_-^2}{2u_t^2}\right)}{4(\eta_-/\sqrt{2}u_t)^3} \right]. \quad (\text{D4})$$

Equation (D4) further is simplified to give

$$D(x, t) \approx \left| \frac{a}{2\pi} \left( \frac{u_t^2}{\eta_-^3 t} \right) \right|^2, \quad \text{for } \eta_- > 0 \text{ and large.} \quad (\text{D5})$$

We find that beyond the front, there is a power-law decay ( $\propto \eta_-^{-6}$ ). We can see that this result [Eq. (D5)] agrees with the numerical simulations [Fig. 5(c)] not only in terms of the exponent of the power law but also in terms of the coefficients given in Eq. (D5).

## 2. Nonintegrable case, $k \neq 2$

### a. $1 < k < 3$

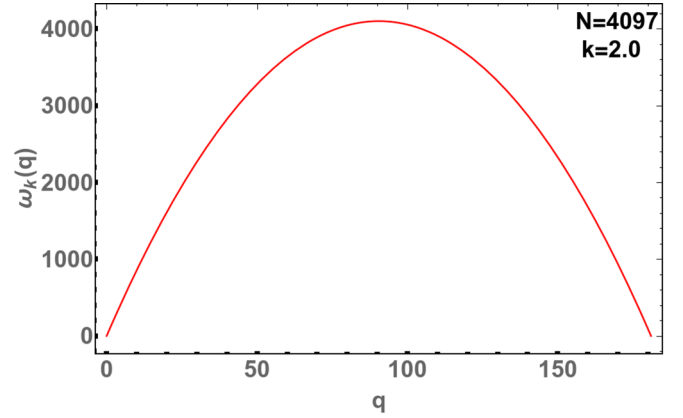
Now turning our attention to the next case, we try to analyze the asymptotic behavior of

$$D_{R,L}(x, t) = \frac{a}{2\pi} \frac{B_k(\Delta_{\mp})}{(3t\beta_k)^{1/k}}, \quad \text{with } \Delta_{k,\mp} = \frac{x \mp \alpha t}{(3t\beta_k)^{1/k}}, \quad (\text{D6})$$

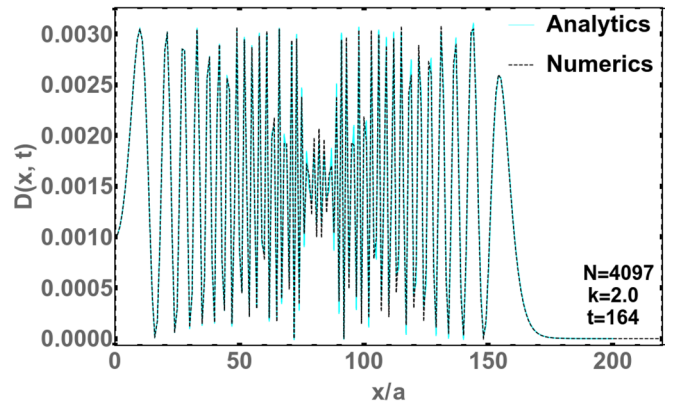
where we define a special function,

$$B_k(y) := \int_0^{(3t\beta_k)^{1/k} \frac{\pi}{a}} ds \cos\left(y s + \frac{s^k}{3}\right). \quad (\text{D7})$$

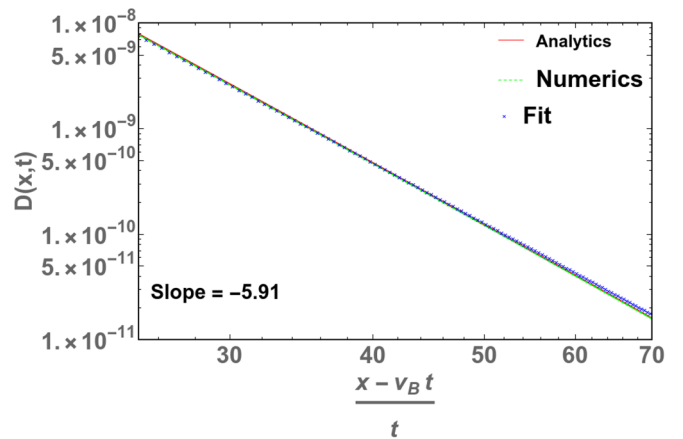
The reader is referred to Eq. (16) to find the definition of  $\Delta_{k,\pm}$  for different values of  $k$ . Again, we are interested in this analysis for large  $N$  (equivalently,  $a \rightarrow 0^+$ ) and large  $\Delta_{k,\mp}$



(a)



(b)



(c)

FIG. 5. (a) Dispersion relation over one time period in  $q$ , for  $k = 2$ ,  $q \in [0, 2\pi/a]$ . (b) Comparing OTOC from direct numerical simulation with the analytical expression at a time snapshot,  $t \approx 164$  (in units of  $a/v_B$ ). Note that, for visualization purposes, we have plotted only the positive  $x$ -axis and the results are mirror symmetric on the other side. (c) Power-law decay of OTOC beyond the cone for  $k = 2$  and  $N = 4097$ . The slope depicts the exponent of the power law. Note that the asymptotics agrees with Eq. (D5) including coefficients. Here  $a \sim 0.0347$ ,  $v_B \sim 90.5207$ .

limits of the system. The strategy would be to again look at the asymptotic form of Eq. (D7). But in the absence of an analytical expression we resort to numerical methods. We find a power-law decay of the form

$$D(x, t) \propto |\Delta_{\pm}^{-(k+1)}|^2, \quad (\text{D8})$$

where  $-/+$  correspond to the right or left sector, respectively. Therefore, the OTOC outside the light cone decays as a power law with exponent  $2k + 2$  [see Fig. 2(c) for  $k = 1.5$ ].

### b. $3 < k < 5$

As we have discussed, just considering the first two terms in the expansion Eq. (B12) does not capture the power-law decay of the OTOC. This is because we effectively end up with the Airy function, which has an exponentially decaying tail. So in order to observe the power-law nature of the OTOC, one has to consider the next-order term in Eq. (B12) as well, in addition to the first two terms.

The expectation is that once the Airy-like behavior of the dominant term washes away, the power-law nature of the subdominant term will take over. This amounts to using Eq. (B12) in Eq. (C4). We find that including the next-order term  $\sim q^k$  recovers the power-law from an Airy-like behavior. For example, this claim about a power-law behavior is verified, for  $k = 4.5$ , by the direct numerical simulations and asymptotic analysis of the OTOC using the full dispersion relation [Eq. (B10)], as is seen in Fig. 4. We find a decay  $\propto |\Delta_{\pm}|^{-11}$  in this case.

Notice the drastic difference in the nature of the envelope of the OTOC profile as one goes from  $k < 2$  (peaking at the center and then having a downward envelope) to  $k = 2$  (essentially flat) and  $k > 2$  (peaking at the edges and having an upward envelope). The integrable model ( $k = 2$ ) serves as a transition point for a change in the nature of propagation of the perturbations through the system.

### c. $k = 3$

The case of  $k = 3$ , and more generally, odd integer values of  $k$  is a little subtle from an analytical analysis stand point. As elaborated in Eq. (B14), the subtle cancellation of divergences arising due to the Riemann  $\zeta$  function and the  $\Gamma$  function gives rise to a logarithm term. This is a crucial term as it gives rise to the power-law decay of the OTOC. As is clear, in the absence of this term, we obtain Airy-like behavior for  $k = 3$ , due to the  $q^3$  term in Eq. (B12). For  $k = 3$ , using Eq. (B12) in Eq. (C4) produces a power-law decay of the OTOC  $\propto |\Delta_{\pm}|^{-8}$ .

These observations strongly suggest that the long-range nature of Riesz gas family of models is what gives rise to the power-law decay of the OTOC (for  $k > 1$ ). A particular term in the expansion of  $\omega_k(q)$  at  $O(q^k)$ ,  $\forall k > 1$  explains the power law.

## APPENDIX E: BROYDEN-FLETCHER-GOLDFARB-SHANNON (BFGS) ALGORITHM

We have implemented the BFGS algorithm [61,62] to find the global minimum energy configuration of our system [Eq. (A1)] for system sizes upto  $N = 4097$ . This is an iterative algorithm which can be used for nonlinear, unconstrained optimization problems. Below we provide the algorithm. Let  $V(\{x_i\})$  [for example, Eq. (A1)] be a scalar function on  $\mathbb{R}^N$  which is to be minimized.  $\nabla V(\{x_i\})$  is the corresponding gradient.  $\mathbf{M}$  is the Hessian matrix [for example, Eq. (A2)].

(1) Make an initial guess for the minimizing configuration  $\mathbf{x}_0 = \{x_i^0\}$ . Using this compute  $\mathbf{M}_0 = \mathbf{M}(\mathbf{x}_0)$  and  $\nabla V_0 = \nabla V(\mathbf{x}_0)$ .

(2) Find the minimizing direction by solving:  $\mathbf{M}_n \mathbf{p}_n = \nabla V_n$ . Here  $\mathbf{p}_n$  is the minimization direction at the  $n$ th iterative step. Therefore, we solve the inverse problem  $\mathbf{p}_n = \mathbf{M}_n^{-1} \nabla V_n$ .

(3) Now, we try to find the optimum step size  $\alpha_n$  to take in the minimization direction. One could use the backtracking line-search method for this purpose. We start with a sufficiently large initial step size  $\alpha_0$  and iteratively reduce it, i.e.,  $\alpha_{j+1} = \eta \alpha_j$  where  $\eta \in (0, 1)$  is a control parameter. This is done until the Armijo-Goldstein condition is satisfied, namely,  $V(\mathbf{x}_n) - V(\mathbf{x}_n + \alpha_j \mathbf{p}_n) > \alpha_j \gamma$ , where  $\gamma = -c\delta$  and  $\delta = \nabla V \cdot \mathbf{p}_n$ . Here similar to  $\eta$ ,  $c \in (0, 1)$  is another control parameter. So we finally find  $\alpha_n$  such that it is the largest of the set  $\alpha'_j$ s until the Armijo-Goldstein condition is still satisfied.

(4) Updating procedure:

(i)  $\mathbf{x}_{n+1} = \mathbf{x}_n + \alpha_n \mathbf{p}_n$

(ii)  $\mathbf{s}_n = \alpha_n \mathbf{p}_n$

(iii)  $\mathbf{y}_n = \nabla V_{n+1} - \nabla V_n$

(iv)  $\mathbf{M}_{n+1} = \mathbf{M}_n + \frac{\mathbf{y}_n \mathbf{y}_n^T}{\mathbf{y}_n^T \mathbf{s}_n} - \frac{\mathbf{M}_n \mathbf{s}_n \mathbf{s}_n^T \mathbf{M}_n^T}{\mathbf{s}_n^T \mathbf{M}_n \mathbf{s}_n}$

(5) Repeat steps 2–4.

## APPENDIX F: A COMPARISON WITH THE TWO-POINT CORRELATOR

The two-point correlator is given by the expression  $\langle x_i(t)x_0(0) \rangle$ , where  $x_i(t)$  is the position of the  $i$ th particle at time  $t$ . On the other hand the classical OTOC is given by  $\langle |\frac{x_i^I(t) - x_i^{II}(t)}{\epsilon}|^2 \rangle$ . Here  $\langle \cdot \rangle$  is the average over a thermal ensemble of initial conditions at a given temperature  $T$ . As mentioned before, for low enough temperatures, we do not need to make an ensemble average.

In our setup,  $x_i^I(0) = y_i$  (except the middle particle position which is perturbed by  $\epsilon$ ). On the other hand, we take  $x_i^{II}(0) = y_i$ . Here  $y_i$  is the equilibrium position of the  $i$ th particle. This immediately implies that  $x_i^{II}(t) = y_i$  at all times. We can now relabel  $x_i^I(t)$  as  $x_i(t)$  and rewrite the OTOC as  $|\frac{x_i(t) - y_i}{\epsilon}|^2$ . In this form, it is apparent that the two-point correlator and the classical OTOC probe similar physics. However, it should be emphasized that this similarity is because of the low-temperature effects. In a more general setup at higher temperatures, the classical OTOC is better suited to probe the perturbations in extended classical systems.

- [1] G. L. Sewell, *Quantum Theory of Collective Phenomena* (Oxford University Press, Oxford, 1989).
- [2] G. Schütz, *Exactly Solvable Models for Many-Body Systems Far from Equilibrium*, edited by C. Domb and J. Lebowitz, Phase Transitions and Critical Phenomena, vol. 19 (Academic Press, Massachusetts, USA, 2001).
- [3] L. F. Cugliandolo, *C. R. Phys.* **14**, 685 (2013).
- [4] K. Kaneko and I. Tsuda, *Complex Systems: Chaos and Beyond: A Constructive Approach with Applications in Life Sciences* (Springer Science & Business Media, Berlin, Heidelberg, Germany, 2011).
- [5] H. Stanley, *Introduction to Phase Transitions and Critical Phenomena* (Oxford University Press, Oxford, 1987).
- [6] O. Babelon, D. Bernard, and M. Talon, *Introduction to Classical Integrable Systems* (Cambridge University Press, Cambridge, England, 2003).
- [7] A. Das, *Integrable Models*, World Scientific Lecture Notes in Physics Vol. 30 (World Scientific, Singapore, 1989).
- [8] M. A. Olshanetsky and A. M. Perelomov, *Phys. Rep.* **71**, 313 (1981).
- [9] M. Olshanetsky and A. Perelomov, *Phys. Rep.* **94**, 313 (1983).
- [10] T. Kinoshita, T. Wenger, and D. S. Weiss, *Nature (London)* **440**, 900 (2006).
- [11] N. Malvania, Y. Zhang, Y. Le, J. Dubail, M. Rigol, and D. S. Weiss, *Science* **373**, 1129 (2021).
- [12] M. Schemmer, I. Bouchoule, B. Doyon, and J. Dubail, *Phys. Rev. Lett.* **122**, 090601 (2019).
- [13] L. Edward, *The Essence of Chaos* (University of Washington Press, Seattle, USA, 1993).
- [14] S. H. Strogatz, *Nonlinear Dynamics and Chaos* (Perseus Books, New York City, USA, 1996).
- [15] M. C. Gutzwiller, *Chaos in Classical and Quantum Mechanics*, vol. 1 (Springer Science & Business Media, New York, USA, 2013).
- [16] F. Haake, in *Quantum Coherence in Mesoscopic Systems*, edited by B. Kramer (Springer, New York, 1991), pp. 583–595.
- [17] D. C. Mattis, *The Many-Body Problem: An Encyclopedia of Exactly Solved Models in One Dimension* (World Scientific, Singapore, 1993).
- [18] A. Dhar, A. Kundu, S. N. Majumdar, S. Sabhapandit, and G. Schehr, *J. Phys. A: Math. Theor.* **51**, 295001 (2018).
- [19] A. Dhar, A. Kundu, S. N. Majumdar, S. Sabhapandit, and G. Schehr, *Phys. Rev. Lett.* **119**, 060601 (2017).
- [20] R. D. H. Rojas, C. S. H. Calva, and I. P. Castillo, *Phys. Rev. E* **98**, 020104(R) (2018).
- [21] F. J. Dyson, *J. Math. Phys.* **3**, 157 (1962).
- [22] F. Calogero, *Lett. Nuovo Cimento (1971–1985)* **13**, 411 (1975).
- [23] F. Calogero, *J. Math. Phys.* **12**, 419 (1971).
- [24] A. P. Polychronakos, *J. Phys. A* **39**, 12793 (2021).
- [25] M. Lu, N. Q. Burdick, S. H. Youn, and B. L. Lev, *Phys. Rev. Lett.* **107**, 190401 (2011).
- [26] A. Griesmaier, J. Werner, S. Hensler, J. Stuhler, and T. Pfau, *Phys. Rev. Lett.* **94**, 160401 (2005).
- [27] J. M. Brown, J. M. Brown, and A. Carrington, *Rotational Spectroscopy of Diatomic Molecules* (Cambridge University Press, Cambridge, England, 2003).
- [28] J. Zhang, G. Pagano, P. W. Hess, A. Kyprianidis, P. Becker, H. Kaplan, A. V. Gorshkov, Z.-X. Gong, and C. Monroe, *Nature (London)* **551**, 601 (2017).
- [29] L. Yan, W. Wan, L. Chen, F. Zhou, S. Gong, X. Tong, and M. Feng, *Sci. Rep.* **6**, 21547 (2016).
- [30] D. H. E. Dubin, *Phys. Rev. E* **55**, 4017 (1997).
- [31] F. D. Cunden, P. Facchi, M. Ligabò, and P. Vivo, *J. Phys. A: Math. Theor.* **51**, 35LT01 (2018).
- [32] M. Riesz, *Acta Sci. Math. Univ. Szeged* **9**, 1 (1938).
- [33] S. Agarwal, A. Dhar, M. Kulkarni, A. Kundu, S. N. Majumdar, D. Mukamel, and G. Schehr, *Phys. Rev. Lett.* **123**, 100603 (2019).
- [34] A. Kumar, M. Kulkarni, and A. Kundu, *Phys. Rev. E* **102**, 032128 (2020).
- [35] M. Kulkarni and A. G. Abanov, *Phys. Rev. A* **86**, 033614 (2012).
- [36] J. A. Joseph, J. E. Thomas, M. Kulkarni, and A. G. Abanov, *Phys. Rev. Lett.* **106**, 150401 (2011).
- [37] Y. Sekino and L. Susskind, *J. High Energy Phys.* **10** (2008) 065.
- [38] S. H. Shenker and D. Stanford, *J. High Energy Phys.* **03** (2014) 067.
- [39] E. B. Rozenbaum, S. Ganeshan, and V. Galitski, *Phys. Rev. Lett.* **118**, 086801 (2017).
- [40] I. Kukuljan, S. Grozdanov, and T. Prosen, *Phys. Rev. B* **96**, 060301(R) (2017).
- [41] A. Bohrdt, C. B. Mendl, M. Endres, and M. Knap, *New J. Phys.* **19**, 063001 (2017).
- [42] A. Lakshminarayan, *Phys. Rev. E* **99**, 012201 (2019).
- [43] V. Khemani, D. A. Huse, and A. Nahum, *Phys. Rev. B* **98**, 144304 (2018).
- [44] A. Das, S. Chakrabarty, A. Dhar, A. Kundu, D. A. Huse, R. Moessner, S. S. Ray, and S. Bhattacharjee, *Phys. Rev. Lett.* **121**, 024101 (2018).
- [45] S. D. Murugan, D. Kumar, S. Bhattacharjee, and S. Sankar Ray, *Phys. Rev. Lett.* **127**, 124501 (2021).
- [46] T. Bilitewski, S. Bhattacharjee, and R. Moessner, *Phys. Rev. Lett.* **121**, 250602 (2018).
- [47] T. Bilitewski, S. Bhattacharjee, and R. Moessner, *Phys. Rev. B* **103**, 174302 (2021).
- [48] M. Kumar, A. Kundu, M. Kulkarni, D. A. Huse, and A. Dhar, *Phys. Rev. E* **102**, 022130 (2020).
- [49] S. Ruidas and S. Banerjee, *arXiv:2007.12708* (2020).
- [50] S. Bera, K. Lokesh, and S. Banerjee, *arXiv:2105.13376* (2021).
- [51] A. K. Chatterjee, M. Kulkarni, and A. Kundu, *arXiv:2106.01267* (2021).
- [52] A. K. Chatterjee, A. Kundu, and M. Kulkarni, *Phys. Rev. E* **102**, 052103 (2020).
- [53] S. Gopalakrishnan, D. A. Huse, V. Khemani, and R. Vasseur, *Phys. Rev. B* **98**, 220303(R) (2018).
- [54] C.-J. Lin and O. I. Motrunich, *Phys. Rev. B* **97**, 144304 (2018).
- [55] C. B. Dağ, L.-M. Duan, and K. Sun, *Phys. Rev. B* **101**, 104415 (2020).
- [56] S. Xu and B. Swingle, *Nat. Phys.* **16**, 199 (2020).
- [57] M. Gärtner, J. G. Bohnet, A. Safavi-Naini, M. L. Wall, J. J. Bollinger, and A. M. Rey, *Nat. Phys.* **13**, 781 (2017).
- [58] A. Erdélyi, W. Magnus, F. Oberhettinger, and F. G. Tricomi, *Higher Transcendental Functions*, Vol. 1 (McGraw-Hill Book Company, Inc., New York-Toronto-London, 1953).

- [59] J. Maldacena, S. H. Shenker, and D. Stanford, *J. High Energy Phys.* **08** (2016) 106.
- [60] S. Agarwal, M. Kulkarni, and A. Dhar, *J. Stat. Phys.* **176**, 1463 (2019).
- [61] R. Fletcher, *Comput. J.* **13**, 317 (1970).
- [62] C. G. Broyden, *IMA J. Appl. Math.* **6**, 76 (1970).
- [63] M. Heyl, F. Pollmann, and B. Dóra, *Phys. Rev. Lett.* **121**, 016801 (2018).
- [64] C. B. Dağ, K. Sun, and L.-M. Duan, *Phys. Rev. Lett.* **123**, 140602 (2019).
- [65] R. J. Lewis-Swan, S. R. Muleady, and A. M. Rey, *Phys. Rev. Lett.* **125**, 240605 (2020).
- [66] G. Benettin, L. Galgani, and J.-M. Strelcyn, *Phys. Rev. A* **14**, 2338 (1976).
- [67] L. Colmenarez and D. J. Luitz, *Phys. Rev. Research* **2**, 043047 (2020).